Influence of Preferential Diffusion in Turbulent Lean Premixed Hydrogen-Rich Syngas Spherical Flames at Elevated Pressure

K.K.J. Ranga Dinesh[*1,] H. Shalaby [1] , K.H. Luo [2] , D. Thévenin [3]
[1]Energy Technology Research Group, Faculty of Engineering and the Environment, University of Southampton, Southampton, SO17 1BJ, UK.
[2]Department of Mechanical Engineering, University College London, Torrington Place, London, WC1E 7JE, UK.
[3]Laboratory of Fluid Dynamics and Technical Flows, University of Magdeburg "Otto von Guericke", Universitatsplatz 2, D-39106 Magdeburg, Germany

Abstract
The objective of this work was to investigate the influence of preferential diffusion on flame structure and propagation of lean-premixed hydrogen-carbon monoxide syngas-air flame at elevated pressure using direct numerical simulation (DNS) and detailed chemistry. The physical problem investigated is lean-premixed H_2/CO outwardly propagating turbulent spherical flame at constant pressure of 4bar and at constant turbulent Reynolds number of 150. It is observed that the local flame structure, heat release rate tangential train rate are strongly altered by preferential molecular diffusion at elevated pressure.

Introduction

Combustion technology is the most important energy conversion method which produces over 80% of the world energy by burning fossil fuels, such as petroleum, coal, and natural gas [1]. However, attention has increasingly turned towards emission control technologies of combustion for the reduction of greenhouse gases (GHGs). In an effort to reduce the GHGs of combustion processes while maintaining high efficiency power generation, development of combustion technology using more environmentally friendly fuels such as high hydrogen content (HHC) syngas becomes important [2]. However, the possibility of burning HHC syngas in modern lean premixed combustion engines can impose challenging constraints which need detailed investigations.

Preferential diffusion [3] is one such important physical phenomenon for HHC lean premixed combustion. Preferential diffusion affects chemical reaction and heat transfer that can play a significant role in hydrogen or hydrogen-rich combustion , and it is often described by the Lewis number, Le , defined as the ratio of thermal to fuel mass diffusivity. In the reacting flow field, non-unity Lewis numbers correspond to the potential presence of preferential diffusion effects, while different values of the species Lewis numbers correspond to differential diffusion effects.

Direct numerical simulation (DNS) in which the complete spectrum of scales is resolved, produces realistic realisation of turbulent combusting flames which can potentially help to identify preferential diffusion effects in turbulent lean premixed high hydrogen content combustion as well as turbulence/chemistry interactions. The integration of DNS and theoretical formulations enables us to analyse the mechanisms in detail to reveal the underlying physics and therefore systematically link the information obtained from numerical simulations to characterise preferential diffusion effects.

The effect of preferential diffusion on hydrogen-air premixed combustion has been investigated in a number of DNS studies. For example, Im and Chen [4] investigated preferenatial diffusion effects on the burning rate of turbulent premixed hydrogen-air flames. Bell et. al. [5] discussed the effect of Lewis number on flame morphology and local flame propagation speed on flame curvature in lean premixed hydrogen turbulent flame. Bisetti et. al. [6] examined the effect of temperature stratitification on the occurance of preferential diffusion during the auto-ignition of lean premixed hydrogen-air mixture. Aspden et. al. [7, 8] investigated characterisation of low Lewis number and the role of Lewis number on flames in the distributed burning regime in turbulent lean premixed hydrogen-air flames. Although much DNS investigations have been carried out for preferential diffusion effects on structure and propagation of hydrogen-air premixed flames at atmospheric pressure, the influence of preferential diffusion on structure and propagation of hydrogen or hydrogen-rich syngas premixed flames at elevated pressure has not been fully investigated. This paper describes DNS investigation of effects of preferential diffusion on flame structure and propagation of lean premixed HHC syngas flame at elevated pressure.

Numerical Details

In test cases considered here, two-dimensional DNS were performed for HHC lean premixed H_2/CO syngas fuel mixture with 70% of H_2 and 30% of CO by volume with an equivalence ratio of 0.7. DNS computations involving complete reaction schemes and multicomponent diffusion models remain extremely demanding in terms of computing time and memory.

[*] Corresponding author: dinesh.kahanda-koralage@soton.ac.uk

The outwardly propagating spherical flame at elevated pressures is adopted as a model flame for the present investigation. The set of governing equations solved in DNS is the time-dependent compressible flow Navier-Stokes equations coupled with detailed chemistry and multi-component transport models. Using the Cartesian tensor notation and ignoring all external forces, the conservation equations solved in DNS read:

Mass conservation:

$$\frac{\partial \rho}{\partial t} + \frac{\partial (\rho u_j)}{\partial x_j} = 0 \tag{1}$$

Momentum conservation:

$$\frac{\partial (\rho u_i)}{\partial t} + \frac{\partial (\rho u_j u_i)}{\partial x_j} = -\frac{\partial p}{\partial x_i} + \frac{\partial \tau_{ij}}{\partial x_j}; \quad i = 1,2,3 \tag{2}$$

Species balance:

$$\frac{\partial (\rho Y_k)}{\partial t} + \frac{\partial \left[\rho (u_j + V_{kj}) Y_k \right]}{\partial x_j} = \dot{\omega}_k; \quad k = 1, N_s \tag{3}$$

Energy conservation:

$$\frac{\partial (\rho e_t)}{\partial t} + \frac{\partial \left[(\rho e_t + p) u_j \right]}{\partial x_j} = -\frac{\partial q_j}{\partial x_j} + \frac{\partial (\tau_{ij} u_j)}{\partial x_i} \tag{4}$$

Equation of state:

$$p = \frac{R}{W} T \tag{5}$$

In Equations (1-5), t stands for time, ρ the mixture density, u_j velocity components in the x_j direction, τ_{ij} stress tensor, e_t total energy per unit mass, p pressure, Y_k the mas fraction of species k, N_s the total number of species, V_{kj} the component of the diffusion velocity of species k in the direction j, $\dot{\omega}_k$ the chemical production rate of species k and q_j the jth-component of the heat flux vector.

It is important to note that we used the skew-symmetric formulation for the convective terms in order to reduce numerical dissipation and increase stability. According to this scheme, the derivative of a general convection term can be written as:

$$\frac{\partial (\rho a u_j)}{\partial x_j} = \frac{1}{2} \frac{\partial (\rho a u_j)}{\partial x_j} + \frac{\partial (\rho u_j)}{\partial x_j} + \frac{\rho u_j}{2} \frac{\partial a}{\partial x_j} \tag{6}$$

In this study an equation is solved explicitly for each and every chemical species with comprehensive detailed chemistry, simultaneously with the Navier-Stokes equations. The chemical kinetic mechanism used in this study is the H_2/CO kinetic scheme developed by Goswami et.al. [9]. This reaction model incorporates the thermodynamic, kinetic, and species transport properties related to elevated pressure H_2 and CO oxidation, consisting of 16 species (CO, HCO, CH_2O, CO_2, H_2O, O_2, O, H, OH, HO_2, H_2, N_2, HE, AR) and 52 individual reactions. Furthremore, we also employed multicomponent diffusion transport models to compute the diffusive processes. To compute the diffusion velocity of species i in the mixture, a detailed model equation without Dufour effect is considered:

$$\boldsymbol{V}_i = -\sum_{k=1}^{N_s} D_{ik} \boldsymbol{d}_k - D_i^T \frac{\nabla T}{T} \tag{7}$$

In Eq. (7), D_{ik} denotes the multi-species diffusion coefficient matrix of species i into species k which depends on all state variables. Symmetric condition, $D_{ik} = D_{ki}$ and the property $\sum_{i=1}^{N_s} Y_i D_{ik} = 0$, k=[1,$N_s$], yield the mass conservation constraint for the species diffusion velocities $\sum_{i=1}^{N_s} Y_i \mathbf{V}_i = 0$. $\mathbf{d}_k$ is a species diffusion driving force vector that takes into account gradients of mole fraction and pressure. In most cases, as in the present study, the pressure-induced diffusion is unused and the external forces $\mathbf{f}_j$ are considered to act equally on all species, resulting simply to $\mathbf{d}_k = \nabla X_k$. D_i^T is the thermal diffusion coefficient of species i while the combined term $D_i^T \nabla T / T$ is the Soret or thermodiffusive effect, which accounts for the diffusion of mass as a result of temperature gradient. It is important to note that Soret effect is considered to be vital in situations where light radicals such as H or H_2 are present, in particular for HHC syngas combustion. To compute the diffusion velocities, one has to accurately determine the binary coefficient via the diffusion matrix, which is computationally expensive. In this study, we consider the Hirschfelder-Curtiss approach [10], whereby an appropriate diffusion coefficient, D_i^* for the species i is given as

$$D_i^* = \frac{(1 - Y_i)}{\sum_{k=1, k \neq i}^{N_s} (X_i / D_{ik})} \tag{8}$$

where D_{ik} is the binary diffusion coefficient which depends only on species pair properties, pressure and temperature and X_i is the mole fraction of species i. The diffusion velocity $\mathbf{V}_i$ for species i is divided into a predictor ($\mathbf{V}_i^*$) and a corrector ($\mathbf{V}_c$) term in order to satisfy the mass conservation, which leads to:

$$\boldsymbol{V}_i = \boldsymbol{V}_i^* + \boldsymbol{V}_c; \quad \boldsymbol{V}_i^* = -D_i^* \frac{\nabla X_i}{X_i}; \quad \boldsymbol{V}_c = \sum_{k=1}^{N_s} Y_k \boldsymbol{V}_k^* \tag{9}$$

However, for unity Lewis number calculation, each species is considered to have the same diffusion

coefficient as heat, and the diffusion coefficient for species i is expressed as:

$$D_i = \frac{\lambda}{\rho C_P} \quad (10)$$

where λ is the mixture-averaged thermal conductivity and C_P the mixture specific heat capacities at constant pressure.

The square box had a length of 1.5×10^{-2} m on each side. The grid resolution was equal to $\Delta x = 9\times10^{-6}$ m , resulting in 1600 and 1600 computational nodes respectively along each spatial direction. A time step of approximately 1.8×10^{-9} s was used for all simulations. An initial temperature of $T_u = 300$K is uniformly distributed across the entire domain.

The full compressible governing equations together with considered thermodynamical relations, chemistry and transport models noted above are solved using the parallel DNS flame solver, Parcomb [11, 12]. The equations are discretised in space on a two-dimensional Cartesian grid with high-order finite difference numerical schemes. Derivatives are computed using centered explicit schemes of order six except at boundaries where the order is progressively reduced to four. Temporal integration is realized with a Runge–Kutta algorithm of order four. A Courant-Friedrichs-Levy (CFL) condition for the convective terms and a Fourier condition pertaining to the diffusion terms are treated to ensure the stability of the explicit integration and determine a suitable time step.

To maintain the constant pressure throughout the simulation, boundary conditions are treated with the help of improved non-reflecting inflow/outflow Navier-Stokes characteristics boundary condition (NSBC) by considering additional terms in the definition of the wave amplitudes, and the relaxation treatment for the transverse gradient terms in analogy with the pressure relaxation [13]. The initial Gaussian temperature profile has been constructed to mimic spark ignition of the mixture using a Gaussian temperature profile. The initial isotropic turbulent velocity field for each case was initialised using a combined approach of digital filtering (DF) [14] and random noise diffusion [15].

To discuss the results between non-unity Lewis number and unity Lewis number at elevated pressure, we carried out two DNS test cases: one DNS test with unity Lewis number, and another DNS test case with non-unity Lewis number, both at constant pressure value of p=4bar, and at constant turbulent Reynolds number of Re_t=50.

Results and Discussion

The objective of the results and discussion is to identify how preferential diffusion (non-unity Lewis number) affects flame characterises at elevated pressure value of p=4bar. For this, we present heat release rates, probability density functions (pdf) of temperature gradient and pdf of tangential strain rates at the flame front.

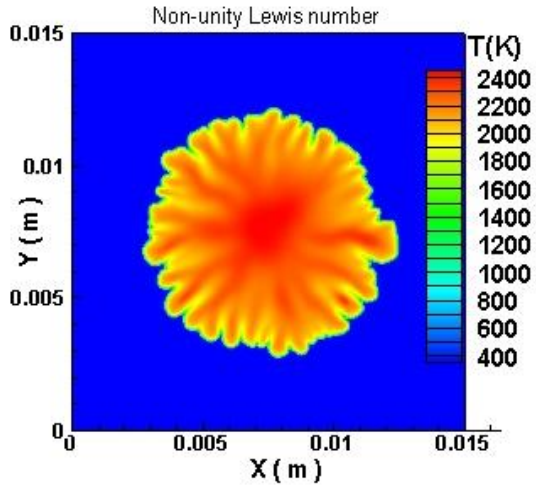

(a)

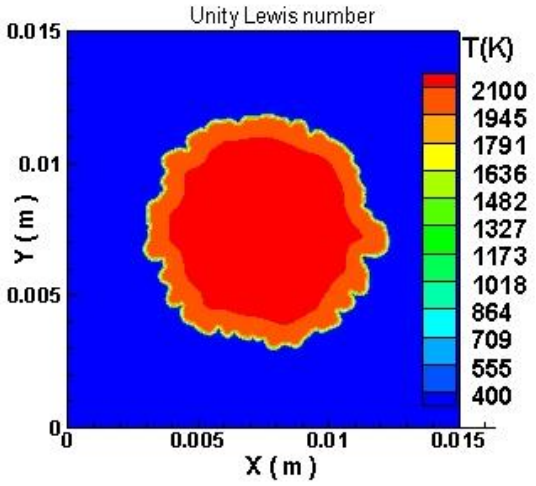

(b)

Fig. 1. Contours of instantaneous flame temperature with (a) non-unity Lewis number and with (b) unity Lewis number at constant turbulent Reynolds number of Re_t=150 and at constant pressure of p=4bar.

Fig. 1 shows comparison of instantaneous snapshot of flame temperature between the non-unity Lewis number case and the unity Lewis number cases at constant elevated pressure value of p=4bar and constant turbulent Reynolds number of Re_t=150. Fig.1 exhibits local increase or reduction of the flame intensity with strong diffusional-thermal cellular instability in the non-unity Lewis number case as a result of significant change of total enthalpy in the gas mixture compared to the unity Lewis number case which is expected to have hydrodynamic cellular instability.

Since H_2 atom is present in large concentration in these flames, its contribution to the total enthalpy of the mixture is significantly contributing to the flame temperature. It is seen from the unity-Lewis number

case that the reaction zone is insensitive to steady straining in the absence of non-unity Lewis number at elevated pressure. This confirms that the strain rate effects remain closely tied to non-unity Lewis number and preferential diffusion effects at elevated pressure value of p=4bar.

As seen in Fig. 2, the scatter of heat release rate display two differences:

(1) the peak heat release rate of the non-unity Lewis number case is about 1.4×10^{11} (Wm^{-3}), while its value for the unity Lewis number case is about 2.5×10^{11} (Wm^{-3});

(2) the scatter of the unity Lewis number case shows more symmetric behaviour compared to non-unity Lewis number case. Furthermore, when preferential diffusion effects are neglected, the peak value of heat release rate and temperature correspond are located at the stoichiometric condition.

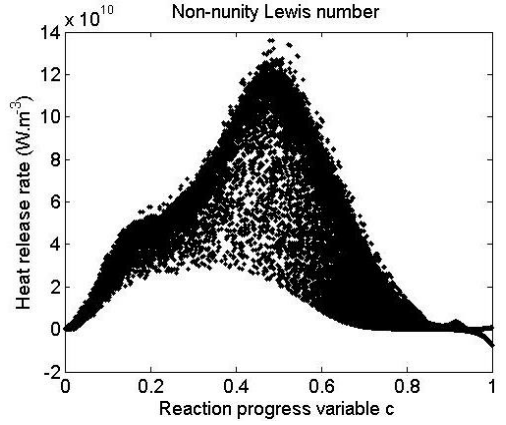

(a)

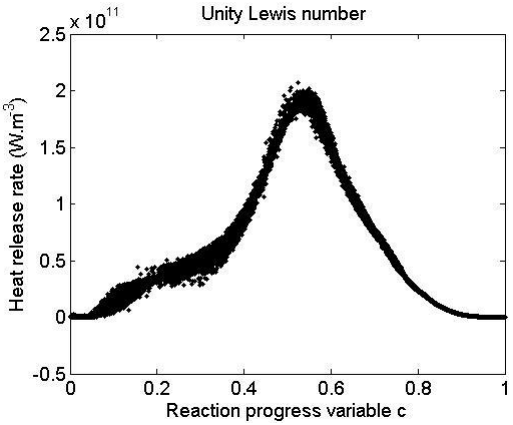

(b)

Fig.2. Scatterplots of heat release rate with (a) non-unity Lewis number and with (b) unity Lewis number (right hand side) at constant turbulent Reynolds number of Re_t=150 and at constant pressure of p=4bar.

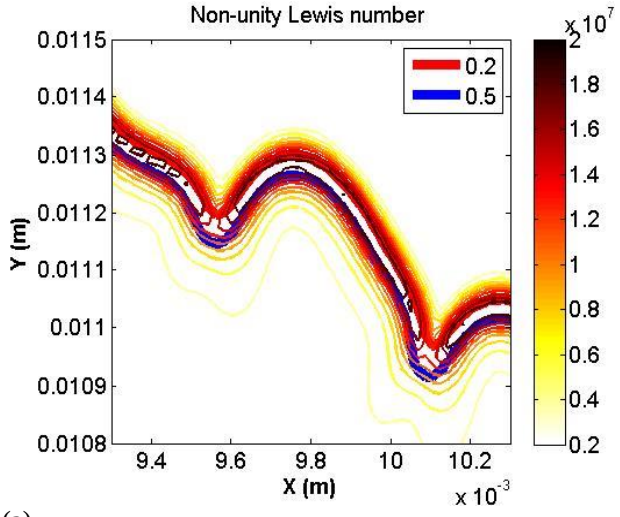

(a)

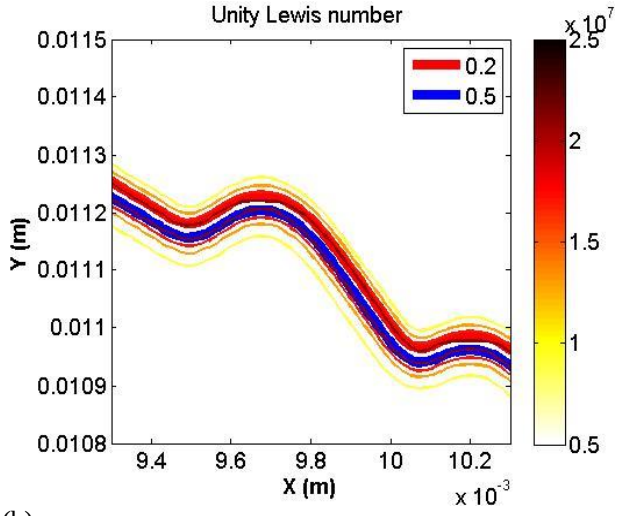

(b)

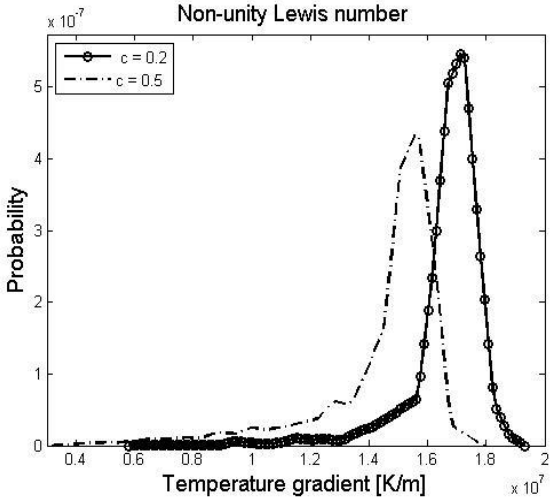

(c)

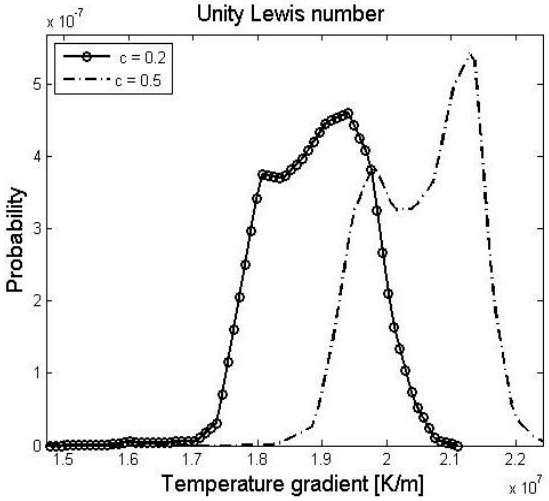

(d)

Fig.3. (a) and (b): Instantaneous temperature gradient field along with the flame front at two different progress variables: c=0.2 and c=0.5; (c) and (d): Probability density functions of temperature gradient conditioned at progress variable c=0.2 and 0.5 with non-unity Lewis number and with unity Lewis number at constant turbulent Reynolds number of Re_t=150 and at constant pressure of p=4bar.

The temperature gradient of the normal temperature profile across the flame front is an important quantity in order to gain an understanding of the instantaneous thermal flame front thickness, and to identify flame thickness trends between unity and non-unity Lewis number cases at elevated pressure. To reveal the influence of non-unity Lewis number on instantaneous thermal flame front thickness at elevated pressure value of p=4bar, changes in the two-dimensional local temperature gradient compared to unity Lewis number were illustrated for two different progress variable values, the preheat zone (c=0.2) and the reaction zone (c=0.5). Fig. 3 (a) and (b) shows instantaneous temperature gradient field at c=0.2 and 0.5, respectively. It is evident from Fig.3 that the temperature gradient field for the non-unity Lewis number case shows more perturbations, steep thermal gradient and much wider flame thickness at the flame front (c=0.5). In the preheat zone (c=0.2), nearly the same behaviour can be identified. The pdfs of the temperature gradient conditioned at these two progress variable values exhibited nearly Gaussian distribution for the non-unity Lewis number case, but deviate slightly towards bimodal distribution for the unity Lewis number case, Fig. 3 (c) and (d).

In addition to temperature gradient and heat release rate, flame stretch can also be used to study the preferential diffusion effects at elevated pressure. This parameter in turn may be written as a sum of contribution of the tangential strain rate and curvature.

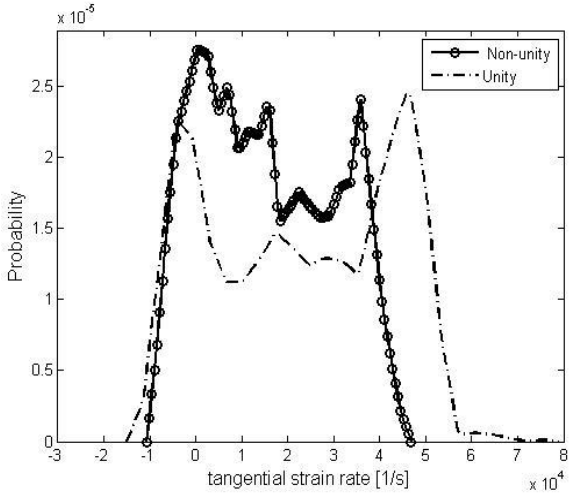

Fig.4. Pdf of tangential strain rate on progress variable iso-value at c=0.5 with non-unity Lewis number and with unity Lewis number at constant turbulent Reynolds number of Re_t=150 and at constant pressure of p=4bar.

To understand the influence of non-unity Lewis numbers on pdf of tangential strain rate and curvature at elevated pressure value of p=4bar, we plotted pdfs of tangential strain rate and mean curvature at c=0.5 (the reaction zone), Fig.4. It is evident from Fig.4 that the strain rate pdfs exhibit a probability of negative tangential strain rate with high peak values for both non-unity and unity Lewis number cases. However, the reduction of pdf of tangential strain rate is depicted for the unity Lewis number case compared to the non-unity Lewis number case. This confirms the reduction of flame front thickness with the low strain rate in the absence of preferential diffusion at elevated pressure.

Conclusions

DNS of turbulent lean premixed high hydrogen content (HHC) H_2/CO syngas flame with detailed chemistry and multi-component transport models has been carried out for outwardly propagating spherical flames in the thin reaction zone regime. Simulations were performed for lean premixed H_2/CO syngas fuel mixture with 70% H_2 and 30% CO by volume with an equivalence ratio of 0.7. It is found that non-unity Lewis number effects play a significant role in the local chemical reaction as well as diffusional-thermal cellular flame structure and heat release rate in the thin reaction zone at elevated pressure of 4bar for turbulent lean premixed HHC H_2/CO syngas flames.

Acknowledgements

This work was sponsored by the Engineering and Physical Sciences Research Council (EPSRC), under the grant EP/L025051/1 (High Hydrogen Content Fuel Burning at High Pressure).

References:

1. BP Statistical Review of World Energy 2012, http://www.bp.com/statisticalreview, 2012
2. T. Lieuwen, V. Yang, R. Yetter, Synthesis gas combustion, CRS Press, Taylor and Francis Group, 2010.
3. M. Matalon, Annu. Rev. Fluid Mech. 39 (2007) 163-191.
4. H.G. Im, J.H. Chen, Combust. Flame 131 (2002) 246-258.
5. J. B. Bell, R. K. Cheng, M.S. Day, I.G. Shepherd, Proc. Combust. Inst. 31 (2007) 1309-1317.
6. F. Bisetti, J.Y. Chen, J.H. Chen, E.R. Hawkes, Proc. Combust. Inst. 32 (2009) 1465-1472.
7. A.J. Aspden, M.S. Day, J.B. Bell, Proc. Combust. Inst. 33 (2011) 1473-1480.
8. A.J. Aspden, M.S. Day, J.B. Bell, Proc. Combust. Inst. 33 (2011) 1463-1471.
9. M. Goswami, R.J.M. Bastiaans, A.A. Konnov, L.P.H. de Goey, Int. J. Hydrogen Energy 39 (2014) 1485-1498.
10. J. Hirschfelder, C. Curtiss, R. Bird, Molecular Theory of Gases and Liquids. Wiley, New York 1954.
11. R. Hilbert, D. Thevenin, Combust. Flame 128 (2002) 22–37.
12. R. Hilbert, F. Tap, H. El-Rabii, D. Thevenin, Prog. Energy Combust. Sci. 30 (2004) 165–193.
13. C.S. Yoo, H.G. Im, Combust. Theory Model. 11 (2007) 259-286.
14. M. Klein, A. Sadiki, J. Janicka, J. Comput. Phys. 186 (2003) 652–665.
15. A. Kempf, M. Klein, J. Janicka, Flow Turbul. Combust. 74 (2005) 67–84.